

Article

Not peer-reviewed version

Influence of Pulsed Interference Laser Heating on Crystallization of amorphous Fe₇₇Cu₁Si₁₃B₉ Ribbons

[Agnieszka Radziszewska](#)* and [Olaf Czyż](#)

Posted Date: 2 April 2024

doi: 10.20944/preprints202404.0201.v1

Keywords: amorphous alloy; pulsed laser interference heating; FeCuSiB ribbons; magnetic field lines; two-dimensional crystallised micro-area



Preprints.org is a free multidiscipline platform providing preprint service that is dedicated to making early versions of research outputs permanently available and citable. Preprints posted at Preprints.org appear in Web of Science, Crossref, Google Scholar, Scilit, Europe PMC.

Copyright: This is an open access article distributed under the Creative Commons Attribution License which permits unrestricted use, distribution, and reproduction in any medium, provided the original work is properly cited.

Article

Influence of Pulsed Interference Laser Heating on Crystallization of Amorphous Fe₇₇Cu₁Si₁₃B₉ Ribbons

Agnieszka Radziszewska ^{1,*} and Olaf Czyż ²

¹ AGH University of Krakow, Faculty of Metals Engineering, al. Mickiewicza 30, 30-059 Krakow, Poland; radzisz@agh.edu.pl

² MAKE IT Olaf Czyż, Zielieniec 61A, 46-034 Pokoj, Poland; o.czyz@o2.pl

* Correspondence: radzisz@agh.edu.pl; Tel.: +48 12 617 44 27

Abstract: The amorphous Fe₇₇Cu₁Si₁₃B₉ ribbons were treated with pulsed laser interference heating (PLIH). It was confirmed here that the use of the laser heating process allowed for obtaining two-dimensional crystallised micro-areas, periodically distributed (at a distance of 17 μm) on the surface of the amorphous ribbons. The correlation between structural changes (SEM, TEM, HRTEM) and the distribution of magnetic field lines of heated amorphous Fe₇₇Cu₁Si₁₃B₉ (FeCuSiB) ribbons is presented. Particular attention is paid to structure changes in micro-areas where, by controlling the laser interference heating process, partial crystallisation of amorphous alloys and the formation of clusters or single nanocrystallites (α-Fe(Si)) embedded in an amorphous matrix are given. The addition of copper to the FeSiB alloy promoted inhibition of grain growth. Electron holography of micro-areas confirmed shifts of the magnetic field lines in the areas of nanocrystallites, the presence of which in the structure caused magnetisation of the surrounding amorphous matrix.

Keywords: amorphous alloy; pulsed laser interference heating; FeCuSiB ribbons; magnetic field lines; two-dimensional crystallised micro-area

1. Introduction

The very rapid continuous development of modern industries is focused on the desire to discover and understand, and in particular the optimization of nanocrystalline soft magnetic materials, in light of their subsequent applications, and taking into account the significant current subject of reducing energy consumption and losses [1–3]. Research is ongoing on new materials with unique soft magnetic properties [4–8]. Since the middle of the twentieth century, there has been a huge increase in interest in nanocrystalline soft magnetic materials, which primarily play a significant role in the production and distribution of energy in the electronics industry, telecommunications, data storage, current and magnetic field sensors [9–12]. Among soft magnetic materials, the largest amounts are alloys of unalloyed iron and FeSiB with the addition of Cu and Nd [13–15]. They influenced significant progress in magnetism, where control of the microstructure and composition of the alloy play a significant role. The benefits of the properties of FeSiB alloys can be achieved as a result of high solidification rates and an optimised annealing process. What distinguishes these types of alloys are their properties. They are characterised by high saturation induction, low magnetic coercivity, high magnetic permeability, and low loss. As a result of their favourable properties, the use of soft magnetic materials is expanding constantly. Produced by Yoshizawa et al. [16], a new alloy (with the composition Fe_{73.5}Nb₃Cu₁Si_{13.5}B₉) has attracted the attention of researchers and industry due to its excellent magnetic soft properties, which are obtained as a result of a properly selected structure. FeCuSiB alloys (in the form of ribbons) are obtained by rapid solidification using the melt spinning technique, which leads to the obtaining of an amorphous structure and the desired properties. At the same time, note that the conventional annealing process of the amorphous phase, leading to the obtaining of nanocrystalline material, is long-lasting and energy-intensive. The furnace annealing of the FeSiB alloy can lead to the formation of the α-Fe(Si) phase with a grain size of

approximately 10 nm [17,18] and the precipitation of Fe₂B, which independently crystallises from the amorphous matrix [3,19,20]. The addition of copper (1%) to the FeSiB alloy, as presented by Yoshizawa [21], to the amorphous phase contributes to the reduction of grain size, resulting in improved soft magnetic properties of the alloy, reduces the crystallisation temperature of the α -Fe phase and provides places for primary crystallisation [2,22,23].

Therefore, the attention paid to FeCuSiB alloys is reflected in the steady increase in the number of publications in the past decades and the great industrial interest in nanocrystalline soft magnetic materials. During alloy crystallisation, as the copper content in the alloy increases, the possibility of the number of nucleation sites increases, which was confirmed by Kulik [23]. At the same time, conventional annealing of amorphous ribbons leads to complete crystallisation, loss of plastic properties, and high brittleness, consequently causing the destruction of the material. This significantly reduces the application of these materials. Indeed, it is necessary to treat the material in such a way that the heating of the ribbons leads to a partially nanocrystalline structure.

However, despite significant progress, to optimise devitrification, microstructure control remains a significant scientific and technological challenge.

To obtain a nanometric structure, very rapid cooling is necessary, at rates of up to $10^5 - 10^6$ K·s⁻¹. One of the most modern surface modification techniques is pulsed laser interference heating (PLIH). So far, the literature has not yet placed much emphasis on the characterisation of the microstructure of FeCuSiB alloy obtained as a result of interference laser heating. This technique enables the change of the structure in micro-areas (dots) with a diameter of 10 μ m, where nanocrystals occur.

The overlap of the incident beams on the material surface causes their interaction and the formation of one-dimensional (lines) and two-dimensional (dots) interference images.

The scientific community is expanding research on FeCuSiB materials because before new materials are developed, it is necessary first to understand the structural changes and magnetic field lines of amorphous Fe₇₇Cu₁Si₁₃B₉ ribbons subjected to local laser surface treatment. Therefore, an important goal of this research is to determine the possibility of creating a nanocrystalline structure in amorphous Fe₇₇Cu₁Si₁₃B₉ ribbons by the interaction of a laser beam, which allows obtaining precisely defined periodically arranged points (62 500) on their surface (5x5 mm) and determining how the structure affects the distribution of magnetic field lines of force.

As part of the work, detailed analyses of structural changes in Fe₇₇Cu₁Si₁₃B₉ ribbons after pulsed laser interference heating (PLIH) were performed using scanning electron microscopy (SEM) and transmission electron microscopy (TEM) techniques, selected area diffraction (SAD), and high-resolution transmission electron microscopy (HRTEM). Electron holography was used to determine local changes in the magnetic field in laser heated micro-areas of the ribbons.

2. Materials and Methods

The materials provided for the research were 35 μ m thick and 10 mm wide amorphous ribbons made of the Fe₇₇Cu₁Si₁₃B₉ alloy obtained by the melt-spinning method. Pulsed laser interference heating was performed using a Q-switch Nd:YAG laser at a laser radiation wavelength of 1064 nm. Laser heating was performed using the basic TEM₀₀ laser mode and the Gaussian energy distribution of the laser beam. The amplification system allowed for a smooth adjustment of the pulse energy from 60 to 470 mJ, with a pulse duration of 10 ns. The interference system consisted of a quartz prism in the shape of a regular tetrahedral pyramid with an apex angle of 172 °. Due to the use of a prism, interference of four laser beams was achieved. This allowed us to obtain a grid of 62 500 laser heated micro-areas on a 5x5 mm surface. To determine surface morphology, the ribbons were electrolytically etched in a 10% solution of chromium III oxide (Cr₂O₃) with water, at a voltage of 10 V and a time of 10 s. Observations were made with a NovaNanoSEM 450 scanning electron microscope (SEM - FEI). SEM analysis was performed in the secondary electron (SE) modes.

Conventional TEM analysis was performed to determine microstructural and phase changes of the ribbons after laser processing using a JEOL JEM 200CX. High-resolution electron microscopy (HRTEM) investigations of nanocrystalline areas embedded in an amorphous structure were carried out using a G2 F20 from Tecnai. High-resolution images were analysed using GATAN Microscopy

Suite software (GMS 3). Thin films for TEM examinations were prepared by cutting 3mm disks from laser-heated areas. Then, thin films were made in two planes: parallel and perpendicular to the heated surface. In order to prepare the thin films in a plane parallel to the heated surface, the disks were ground from the heated side to remove the roughness created during laser heating. In the next step, the disks were mechanically polished in the central part on the laser untreated side, using a GATAN 656 dimpler. After dimpling, the disks were electro-polished using a STUERS TenuPol-5 polishing machine. The polishing reagent was a 5% solution of perchloric acid (HClO_4) in ethanol, the voltage was $U=38-41$ V and the temperature below -24 °C. The disks were then cleaned using a Leica EM RES101 ion milling machine or PIPS from GATAN applying the following parameters: gun voltage $U=3$ keV, gun angle -3° . This thin film preparation allowed us to analyse the changes in structure in the area marked with a red line in Figure 1.

To prepare thin films in a plane perpendicular to the heated surface, lamellas were cut from the dot area using a focused ion beam (FIB) using SEM-FIB Quanta 3D from FEI (Figure 2).

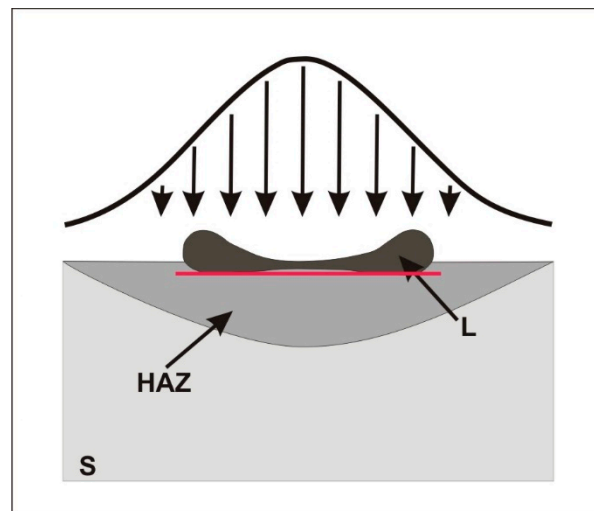


Figure 1. Position of the thin foil (red line) parallel to the laser heated surface. Abbreviations of symbols: L - liquid, S - solid, HAZ - heat affected zone.

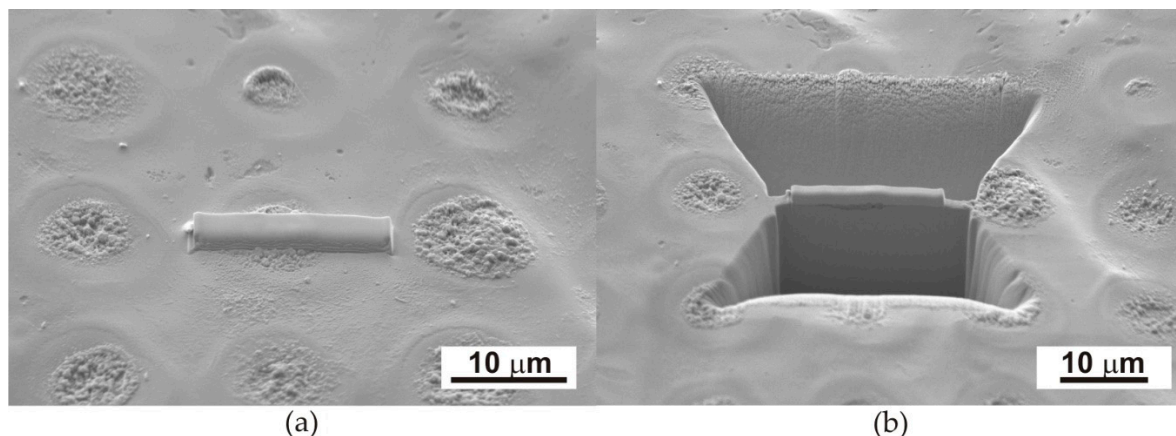


Figure 2. Scanning electron microscopy images showing the periodic dots distributed on the surface of the $\text{Fe}_{77}\text{Cu}_1\text{Si}_{13}\text{B}_9$ ribbon and the steps of lamella preparation – a, b using the FIB method.

Electron holography made it possible to determine the distribution of magnetic field lines in laser heated micro-areas. Therefore, the study was carried out using an HRTEM FEI Titan CUBED 80-300 microscope on thin foils, using the Lorentz mode. Additionally, electron holograms were also analysed when a magnetic field was excited with an objective lens by flowing $\pm 10\%$ of the maximum current.

3. Results

3.1. Microstructural Characterization

3.1.1. Scanning Electron Microscopy Examinations

The pulsed interference interaction of the laser beam with the amorphous ribbon led to the formation of periodically arranged micro-areas on a 5x5 mm surface, consisting of 62,500 dots. The periodic distribution of dots, obtained by laser heating with an energy of 120 mJ and a pulse number of 500, is shown in Figure 3 using the scanning electron microscope. Observations using a scanning electron microscope showed a two-dimensional structure of periodically distributed laser heated micro-areas at a distance of approximately $\Lambda = 17 \mu\text{m}$. The diameter of the dots was approximately $10 \mu\text{m}$ (Figure 3).

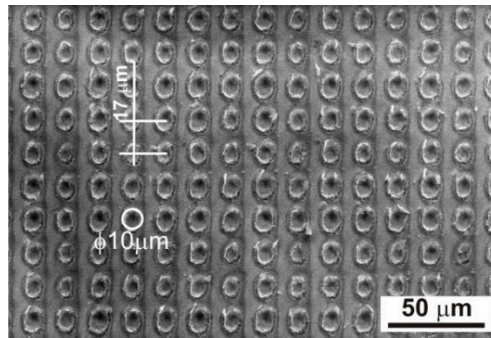


Figure 3. The SEM image shows regularly distributed dots formed on the surface of the $\text{Fe}_{77}\text{Cu}_1\text{Si}_{13}\text{B}_9$ ribbon laser heated with an energy of 120 mJ and a number of pulses of 500.

The increase in the number of laser pulses and energy led to the formation of a more macroscopically visible interference pattern on the surface of the amorphous ribbon, and are shown in Figure 4.

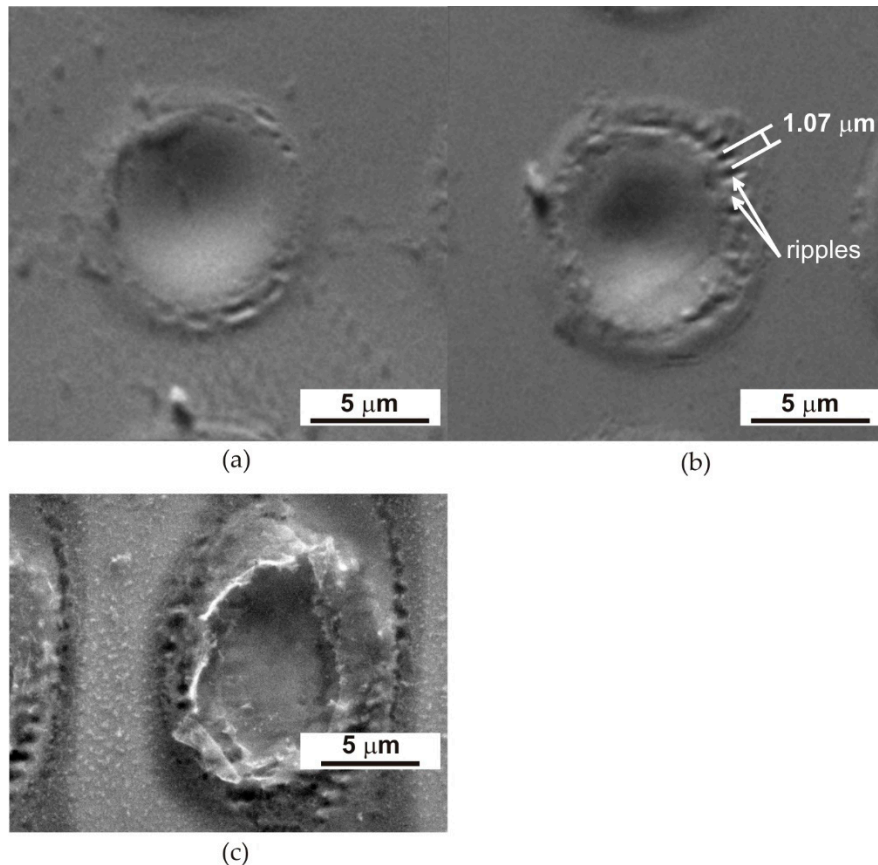


Figure 4. SEM images of the surface of the $\text{Fe}_{77}\text{Cu}_1\text{Si}_{13}\text{B}_9$ ribbon after pulsed laser interference heating with an energy of 120 mJ and a variable number of pulses: a) 200; b) 500 and c) an energy of 170 mJ and 10 pulses.

The structural changes created on the surface of $\text{Fe}_{77}\text{Cu}_1\text{Si}_{13}\text{B}_9$ ribbons resulting from the use of variable energy and the number of pulses correspond to our previous results obtained for FeSiB [6,24]. Therefore, the use of a small number of pulses (10) and a lower beam energy (60-100 mJ) to heat the amorphous ribbon leads to the effect of heating its surface to a ribbon thickness of approximately 100 nm. However, increasing the energy to 120 mJ and a larger number of pulses resulted in melting of the ribbon surface, and at the same time evaporation of the material in micro-areas occurred (Figure 4a,b). Heating with a higher energy of the laser beam (above 170 mJ) was responsible for melting of the material, its partial ablation (evaporation), and deformation of the edges of the heated micro-areas (Figure 4c). Note that the energy distribution in the laser beam is Gaussian, which affects the concentric distribution of individual zones of the structure (Figure 4). The highest energy occurs in the centre of the beam cross-section and decreases along its radius, causing a change in the structure in individual micro-areas. It is clearly visible that in the central part of the dot, with a smaller number of pulses of 200 and an energy of 120 mJ (Figure 4a), the phenomenon of melting and 'pushing' of liquid material into the edge zones of the dot arises as a result of the dynamics of the process, the action of the shock wave and the centrifugal force. As a result, an outflow of liquid material can be seen at the edges of the dots, as shown in Figure 1. At the same time, it should be noted that, in the centre of the dot, the molten material has the highest temperature and is therefore the rarest, which facilitates its movement. If the number of pulses is higher (500) (Figure 4b), characteristic coarse ripples are formed [25], and they are the result of interference between the incident light of the laser beam and the surface scattering wave [25–27]. The period of the observed coarse ripples is close to the wavelength (1,064 μm) of the incident Nd:YAG laser radiation ($\sim 1.07 \mu\text{m}$) (Figure 4b).

Due to the structural effects presented above, the following sections of the TEM results will present a ribbon heated with a laser beam energy of 120 mJ and 500 pulses.

3.1.2. TEM and HRTEM Examinations

Observations using transmission electron microscopy showed the presence of a crystalline structure in the laser heated micro-areas (Figure 5). Figure 5 shows TEM (BF) images in cross-section perpendicular to the ribbon surface of a single laser heated micro-area of the $\text{Fe}_{77}\text{Cu}_1\text{Si}_{13}\text{B}_9$ ribbon. Due to the appearance of a temperature gradient in the areas heated by the laser beam, structural changes were observed in which four zones can be distinguished (Figure 5a). In the first zone, nanocrystalline grains are visible in the centre of the micro-area, around which zone 2 was formed. This zone was in contact with the liquid material, so the temperature reached was higher than in zone 1, resulting in grain growth. Subsequently, zone 3 with an amorphous structure ($\alpha\text{-Fe}(\text{Si})$ phase) is present in the area of the solidified liquid, while in the peripheral area (zone 4) the grains were reduced to nanometric size (Figure 5b). In this zone, single nanocrystals ($\sim 10 \text{ nm}$) and their clusters (Figure 5b) surrounded by an amorphous matrix were observed. The existence of an amorphous structure of the ribbon was confirmed by annular electron diffraction with a small number of reflections from crystallised areas (inset in Figure 5b). The addition of copper to the FeSiB alloy, the initiation of crystallisation using laser heating and immediate cooling facilitate the saturation of the structure with nanocrystallites $\alpha\text{-Fe}(\text{Si})$. Furthermore, Cu segregates to the grain boundaries and blocks its growth, which was confirmed by Kulik's results and other researchers [22,23,28].

Note that laser heating led to the initiation of the formation of crystalline areas, but too short a laser treatment time allowed only a slight increase in the recrystalline phase. This resulted in the formation of a structure composed of a large number of nanometric crystallites (Figure 5) that is not possible to obtain during traditional thermal treatment. The nanocrystalline structure enables the improvement of soft magnetic properties through low magnetic loss due to magnetisation reversal, high magnetic permeability, and low magnetostriction [29–31].

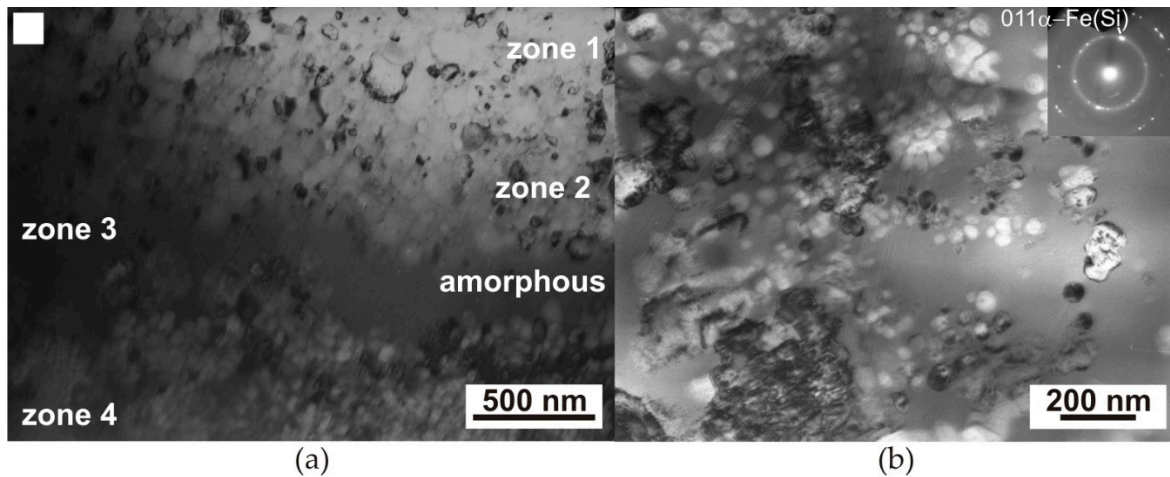


Figure 5. TEM plane view image of a $\text{Fe}_{77}\text{Cu}_1\text{Si}_{13}\text{B}_9$ ribbon laser heated with an energy of 120 mJ and 500 laser pulses, view of the central part of the micro-area/dot; a) general view; b) a peripheral zone - single and clusters of nanocrystals surrounded by an amorphous matrix.

Laser heating of the $\text{Fe}_{77}\text{Cu}_1\text{Si}_{13}\text{B}_9$ alloy with an energy of 120 mJ and a large number of laser pulses (500) in the peripheral areas of the dots led to the formation of clusters of nanocrystallites in an amorphous matrix (Figure 6).

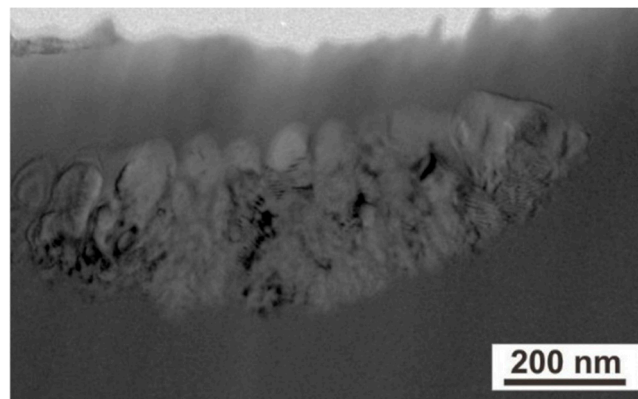


Figure 6. TEM image of a $\text{Fe}_{77}\text{Cu}_1\text{Si}_{13}\text{B}_9$ ribbon cross-section heated with a laser, showing a group of nanocrystallites in an amorphous matrix in the peripheral zone of the dot.

The Fast Fourier transform (FFT) of the area of the partially crystallised amorphous matrix indicates the presence of an $\alpha\text{-Fe(Si)}$ with a large amount of amorphous matrix (Figure 7). High-resolution transmission microscopy of the ribbons revealed the occurrence of an amorphous structure, confirmed by the presence of a halo ring shown in the fast Fourier transform (Figure 7c). The supply of energy, as a result of heating the material with a laser beam, contributed to the partial crystallisation of the amorphous matrix in the area of the boundary with the crystallites (Figure 7b). High resolution TEM observations revealed a structure composed of nanocrystallites areas of the $\alpha\text{-Fe(Si)}$ phase with orientation [001] in an amorphous matrix (Figure 7c).

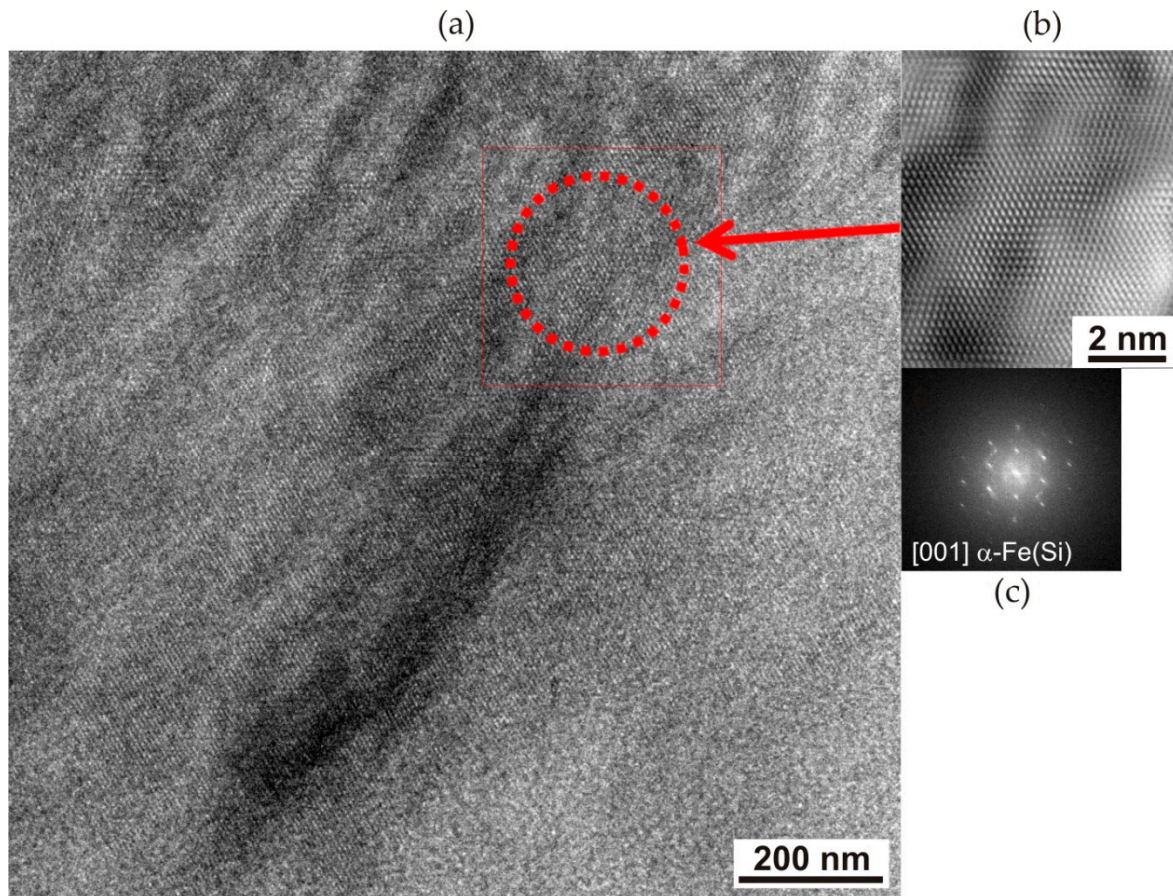


Figure 7. HRTEM image of a $\text{Fe}_{77}\text{Cu}_1\text{Si}_{13}\text{B}_9$ ribbon heated with an energy of 120 mJ and 500 laser pulses: a) general view; b) enlargement of the selected area from Figure 6a; c) FFT from Figure 6a.

3.1.3. Electron Holography: Distribution of Magnetic Force Line

The use of electron holography made it possible to determine local changes in the magnetic field (contours of the solid magnetic phase) in an amorphous material $\text{Fe}_{77}\text{Cu}_1\text{Si}_{13}\text{B}_9$ ribbons crystallised as a result of pulsed interference laser heating, which were performed using a TEM FEI Titan CUBED 80-300 using the Lorentz mode. The samples were prepared in thin foils for TEM. Holograms were obtained by applying the sample configuration: "upside - downside", so first a hologram of the sample was performed in the upper configuration (upside), then a hologram of the sample was created, which was rotated by 180° (downside configuration) relative to the holder axis in the microscope. The obtained holograms were computer processed using the PyHoLo programme (Morawiec et al., 2020), which is necessary to separate the phase shift caused by electrostatic and magnetic field forces, and was used to determine the magnetic nature of the laser heated areas. The reader can learn the basics of this technique, which are presented in Midgley's work (Midgley, 2001).

Figure 8a shows a hologram of the selected peripheral area of the dot in a plane perpendicular to the heating surface (Figure 6) with grouped nanocrystallites embedded in an amorphous matrix.

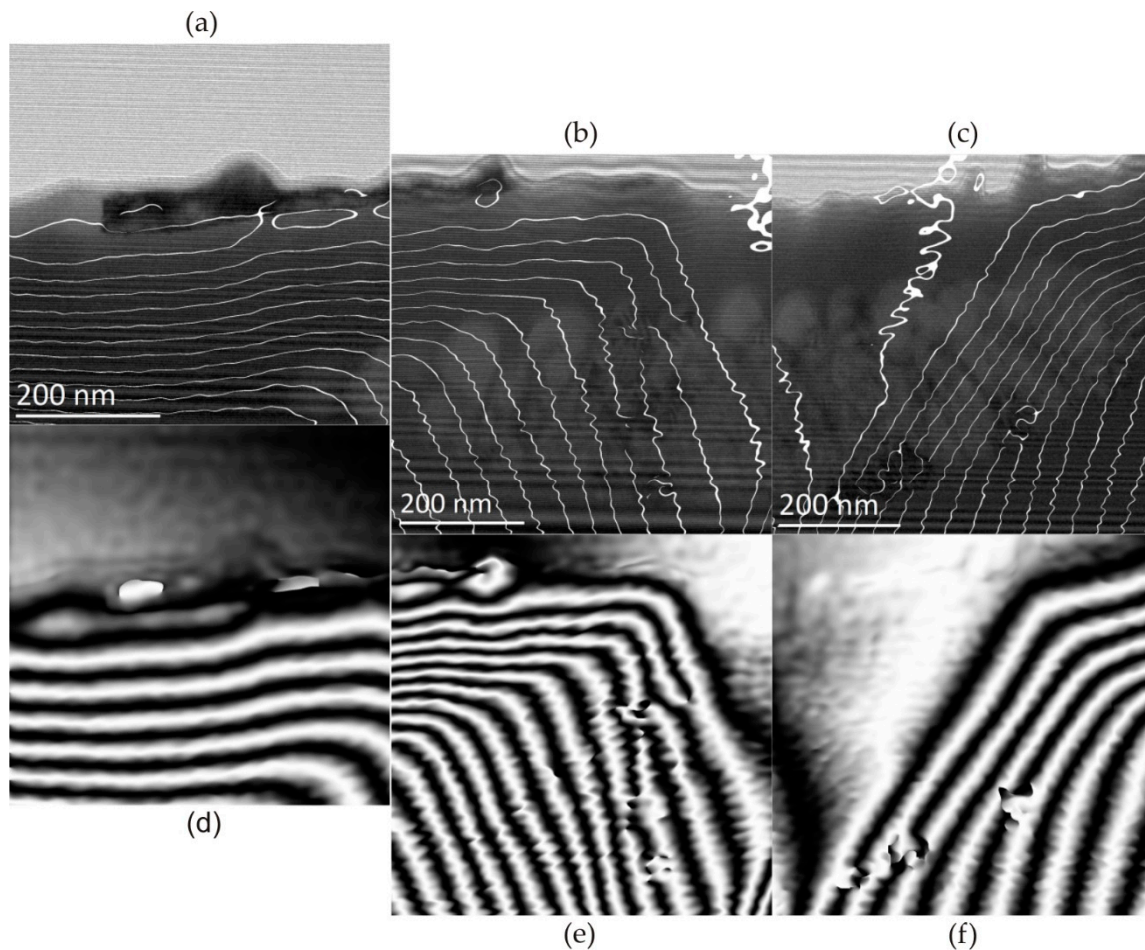


Figure 8. The images show the electron holograms acquired for the $\text{Fe}_{77}\text{Cu}_1\text{Si}_{13}\text{B}_9$ ribbon after laser heating in the absence of an external field. The magnetic field lines are shown: a) in the amorphous matrix; b)-c) phase shift of the magnetic field lines (B) in the area of nanocrystallite clusters, in the absence of magnetic field excitation (H); d)-f) superimposed images of magnetic field lines into a microscopic image. The image refers to the isolated area in Figure 5. Nanocrystallites ($\alpha\text{-Fe}(\text{Si})$) disrupt the position of field force lines.

In Figure 8 changes in the magnetic field lines of force depending on the applied magnetic field are shown. In the absence of an external magnetic field, the recorded hologram, in the area of the amorphous matrix, shows characteristically parallel lines of magnetic field to the edge of the sample (Figure 8a). In turn, the bending of the magnetic field lines occurred in the area of the crystalline phase (Figure 8b,c). Therefore, crystallites cause a step change in the magnetic induction vector. This is due to magnetocrystalline anisotropy, i.e. the presence of crystal axes of easy and hard directions of magnetisation. In this case, the axis of easy magnetisation of the crystalline phase was directed perpendicularly to the edge of the sample. In the observed area, local discontinuities in the field force lines are also visible, which may be caused by the presence of crystallites with different crystallographic orientation.

Additionally, studies of the distribution of magnetic field forces in micro-areas of the laser heated $\text{Fe}_{77}\text{Cu}_1\text{Si}_{13}\text{B}_9$ ribbons were carried out using an external magnetic field. Electron holograms were obtained by inducing a magnetic field with the objective lens of a microscope by flowing +/- 10% of the maximum lens current. Two types of excitation were performed using the direction of current flow: clockwise (+10%) and anticlockwise (-10%). The recorded electron holograms of the $\text{Fe}_{77}\text{Cu}_1\text{Si}_{13}\text{B}_9$ sample subjected to a magnetic field are shown in Figure 9. Figures 9b-f show holograms recorded according to the following excitation plan with objective lenses: initial state - 0% excitation (Figure 9b), with + 10% excitation (Figure 9c), without excitation - 0% (Figure 9d), with excitation - 10% (Figure 9e), without excitation (Figure 9f).

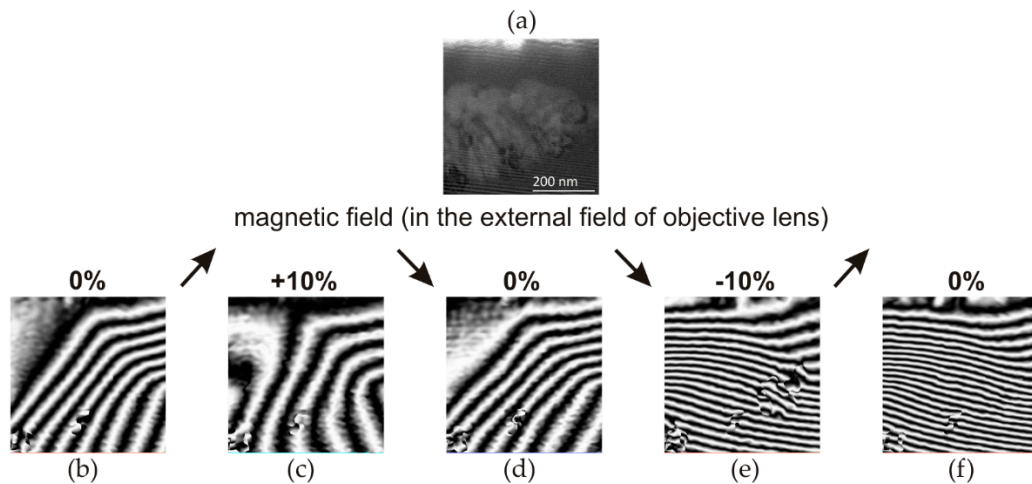


Figure 9. Images showing electron holograms of the $\text{Fe}_{77}\text{Cu}_1\text{Si}_{13}\text{B}_9$ ribbon after laser heating, recorded using an external variable magnetic field, obtained by objective lenses and by applying an excitation of +/-10%. (+) and (-) correspond to the direction of current flow. a) HRTEM image of nanocrystallite clusters in an amorphous matrix. Holograms correspond to: b) no external field; c) +10%; d) 0%; e)-10%; and f) 0% - no external field.

Considering the magnetisation with a positive magnetic field (+10%), one should notice a slight change in the distribution of magnetic-field forces (Figure 9c). However, the distance between the lines changed and therefore the value of the magnetic field changed. After the external magnetic field (Figure 9d), the sample returned to its initial state (Figure 9b). In the next step, the application of an external magnetic field with the opposite direction (negative (-10%) of the current flow) resulted in the remagnetization of both the amorphous matrix and the crystallite clusters (Figure 9e). There was a change in the direction of the magnetic field, and its intensity increased, observed through a changing the arrangement of magnetic force line in crystalline areas. The shutoff of the external magnetic field (Figure 9f) resulted in the return of the characteristic magnetisation of the foil to the level characteristic of the initial state. This means that the external magnetic field generated at -10% excitation led to strong overmagnetization of the amorphous matrix as well as the nanocrystallites. It should be stated that the distributions of the magnetic field lines of force created in the absence of lens excitation (0%) show the magnetic remanence of the material (Figure 9b,d,f). Moreover, as can be seen, the remanence after negative excitation with lenses (-10%) is characterised by a much stronger magnetisation of the matrix. The analyses of the results lead to the conclusion that the easy direction of magnetisation of crystallites is probably such that the external magnetic field created at +10% excitation does not cause their magnetisation. Only the amorphous matrix is magnetised and returns to its initial state after the magnetic field is turned off. In the case of a field created by negative excitation of the lens, both the matrix and the crystallites are magnetised. After the magnetic field, even when the matrix magnetisation disappears, the crystallites remain magnetised, and they are probably the ones that magnetise the matrix.

4. Discussion

The influence of pulsed laser interference heating (PLIH) on the change in the microstructure characteristics of the surface and near-surface areas of an amorphous $\text{Fe}_{77}\text{Cu}_1\text{Si}_{13}\text{B}_9$ ribbon is presented. Our research shows that the advantage of PLIH is the ability to heat specific areas of the ribbon surface in a very short time of laser beam operation. Laser heating of amorphous $\text{Fe}_{77}\text{Cu}_1\text{Si}_{13}\text{B}_9$ ribbons allowed the simple and rapid creation of 62 500 dots with a diameter of approximately 10 μm , periodically arranged (at a distance of $\Lambda = 17 \mu\text{m}$) on their surface (Figure 3).

The laser beam is characterised by a Gaussian energy distribution; thus, the highest temperature is reached in its centre and decreases with the distance from its centre to the amorphous matrix. This results in structural changes obtained in each of the 62,500 dots.

SEM observations of the ribbon surface after laser heating showed that the use of the lowest energy and the number of laser beam pulses led only to the heating of very thin surface layers of the ribbons (up to 100 nm in depth). The increase in energy (above 120 mJ) and the number of pulses above 200 (Figure 4a) resulted in the accumulation of energy in the heated micro-areas, leading to melting and ablation of the material. Explosive evaporation of the material occurs as a consequence of exceeding the ablation threshold. However, heating the laser beam with energy above 170 mJ (Figure 4c), regardless of the number of pulses, led to melting, laser ablation and, in particular. The interaction of the laser beam with the ribbon material led to high temperatures reaching the solidus range only in its thin subsurface layer and crystallisation of the material to a depth of 350 nm.

In the process of preparing thin foil, the material was cut in a plane parallel to the laser heated surface of the ribbon, and ground on the heated side due to its greater surface roughness obtained as a result of the impact of the laser beam. Then its central part was electrolytically polished and the ion cleaned. The position of the thin foil in relation to the zones formed during heating is shown in Figure 2 (red line). As a result, thin foil cut through four characteristic zones in cross-section (Figure 5): 1. centre of the dot, where nucleation and growth of the crystalline phase occurred, resulting in a granular structure; 2. edge, where the crystallite growth rate was higher than the nucleation rate, leading to the formation of a coarse-grained structure; 3. a ring which was quickly melted and cooled and in which the material amorphized; 4. The edge where the nucleation of a large number of crystallites was evenly distributed in the amorphous matrix. The occurrence of these zones is determined by the Gaussian distribution of energy in the laser beam, which leads to the formation of a temperature gradient from the central zone of the micro-area to its peripheral zone. In the middle zone, an increase in the number of pulses led to an increase in the amount of accumulated heat, which promoted the formation of a large number of crystal nuclei and led to the formation of a structure with a grain size of approximately 50-250 nm (Figure 5a) [4,32,33]. The formation of a large number of crystallites led to the mutual blocking of their growth, and thus to a coarse-grained structure.

As we moved away from the centre of the micro-area, the amount of energy decreased, resulting in fewer crystallisation nuclei being formed, and heating with subsequent pulses promoted their growth (grains up to approximately 1 μm were formed - zone 2, Figure 5a). A zone with an amorphous structure was formed around this zone (Figure 5a), and in the farthest peripheral zone, single or nanocrystallite clusters were formed, which were surrounded by an amorphous phase (Figure 5b). The probable mechanism for the formation of the amorphous structure is the accumulation of liquid material in this area, transferred by the shock wave (under the influence of centrifugal force) from the central part of the micro-area melted by the laser beam. The accumulation of liquid material, as a result of heat conduction, could lead to deeper melting of the ribbon in this area, and after the heating cycle stopped, it could lead to its vitrification again [32].

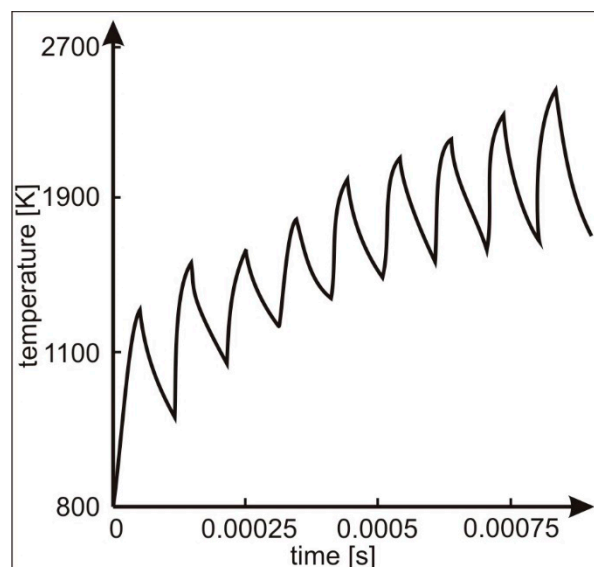


Figure 10. Scheme of surface temperature change in the pulsed laser heated micro-area. Based on [32].

Similar structural changes were also discovered in our previous structure obtained in FeSiB ribbons [6,24]. The presence of copper in the $\text{Fe}_{77}\text{Cu}_1\text{Si}_{13}\text{B}_9$ alloy led to conditions that favoured nucleation rather than the growth of existing grains, as confirmed by Kulik [23].

Due to the rapid heating of the material, the temperatures for the transformations in the solid state increase and rapid solidification (a large number of crystallisation nuclei) allows the formation of a crystalline structure composed of $\alpha\text{-Fe(Si)}$ crystals (Figures 4b and 5). At the same time, copper plays a decisive role in the determination of nanocrystalline microstructures. The addition of copper to the FeSiB alloy causes chemical heterogeneity by forming clusters of Cu atoms, thus providing a high density of nucleation sites in the first stage of crystallisation of $\alpha\text{-Fe(Si)}$ nanocrystallites. During the impact of the laser beam, when the surface temperature of the ribbon increased to solidus temperature, the material was heated to high temperatures and crystallisation of the amorphous structure occurred, resulting in the formation of nanocrystallites ($\alpha\text{-Fe(Si)}$) (Figure 6). At the same time, the short duration of the pulse and the cooling of the material lead to a sudden "freezing" of the structure. Furthermore, the action of subsequent shots causes the nucleation of new nanocrystalline grains without visible growth of the previously formed grains. It should be noted that at the same time, in the case of the FeSiB alloy without the addition of copper, the increase in energy and the number of pulses led to energy accumulation and, consequently, to grain growth [4–6].

Our research highlighted the importance of electron holography (Figure 7), which was used to determine the nanoscale distribution of magnetic field lines in the micro-areas of laser heated amorphous $\text{Fe}_{77}\text{Cu}_1\text{Si}_{13}\text{B}_9$ ribbons. The research was carried out using an HRTEM FEI Titan CUBED 80-300 microscope in Lorentz mode.

The structural changes that occur in the surface layers of $\text{Fe}_{77}\text{Cu}_1\text{Si}_{13}\text{B}_9$ ribbons as a result of the impact of PLIH influenced the distribution of the magnetic field lines of force (Figure 8). There was slight deflection of the magnetic field lines in the areas of small crystallites ($\alpha\text{-Fe(Si)}$) embedded in the amorphous $\text{Fe}_{77}\text{Cu}_1\text{Si}_{13}\text{B}_9$ matrix. Magnetisation with a positive magnetic field (clockwise +10%) allowed only a slight change in the distribution of magnetic field force lines and low magnetisation of the crystallites and the amorphous matrix. Therefore, it should be concluded that the easy direction of the magnetisation of the crystallites is different with positive excitation; therefore, the +10% excitation did not cause their magnetisation (Figure 8c). However, excitation with a negative magnetic field led to strong overmagnetization of the nanocrystallites and the amorphous matrix (Figure 8e). The matrix was then magnetised as a result of the application of an external magnetic field (excitation by the objective lenses of the microscope), as well as by the crystallites present in it.

5. Conclusions

The results of the conducted research broaden our understanding of determining the impact of pulsed laser interference heating on the formation of amorphous $\text{Fe}_{77}\text{Cu}_1\text{Si}_{13}\text{B}_9$ ribbons. The following conclusions can be drawn from the results obtained from the studies.

Favourable selective laser heating of ribbon in a very short time led to the creation of periodically arranged micro-areas composed of 62,500 dots.

Laser heating contributed to structural changes in the ribbon on the surface of 17 μm and in the near-surface areas reaching into the ribbon approximately 350 nm.

The initiation of crystallisation as a result of the impact of the laser beam on the amorphous $\text{Fe}_{77}\text{Cu}_1\text{Si}_{13}\text{B}_9$ ribbon and the rapid cooling allow the structure to be saturated with $\alpha\text{-Fe(Si)}$ nanocrystallites.

The addition of copper to the FeSiB alloy promoted the nucleation of new crystallites (approximately 10 nm in size) in the amorphous matrix.

Laser heating caused crystallisation of the amorphous matrix and the formation of $\alpha\text{-Fe(Si)}$ nanocrystallites with a size of approximately 10 nm and an orientation [001].

Changes in the distribution of the magnetic field line force occurred in the areas of α -Fe(Si) nanocrystallites.

Author Contributions: Conceptualization, A.R., O.Cz.; methodology, A.R., O.Cz.; investigation, O.Cz.; writing—original draft preparation, A.R.; writing—review and editing, A.R.; visualization, A.R., O.Cz.; supervision, A.R. All authors have read and agreed to the published version of the manuscript.

Funding: This research was funded by the AGH University of Krakow (contract number: 16.16.110.663) and the National Science Centre (NCN) of Poland (contract number: OPUS 10, UMO-2015/19/B/ST8/01070).

Institutional Review Board Statement: Not applicable.

Informed Consent Statement: Not applicable.

Data Availability Statement: Not applicable.

Acknowledgments: The authors acknowledge Piotr Dłużewski and Roman Ostrowski for assistance in this research work.

Conflicts of Interest: The authors declare no conflicts of interest.

References

- Hasegawa, N.; Saito, M. Structural and soft magnetic properties of nanocrystalline (Fe, Co, Ni)-Ta-C films with high thermal stability. *Journal of Magnetism and Magnetic Materials* **1992**, *103*, 274-284.
- Herzer, G. Modern soft magnets: Amorphous and nanocrystalline materials. *Acta Materialia* **2013**, *61*, 718-734.
- Suzuki, K.; Herzer, G. Soft magnetic nanostructures and applications. *Advanced Magnetic Nanostructures* **2006**, 365-401.
- Czyz, O.; Kusinski, J.; Radziszewska, A.; Ostrowski, R.; Morgiel, J.; Kanak, J.; Kac, M. Modification of the structure and properties of FeSiB amorphous ribbon by interference pulsed laser heating. *Archives of Metallurgy and Materials* **2018**, *63*, 2001-2007. <https://doi.org/10.24425/amm.2018.125136>.
- Kusinski, J.; Czyz, O.; Radziszewska, A.; Stobiecki, T.; Ostrowski, R.; Strzelec, M.; Kac, M. Pulsed interference laser heating of amorphous FeSiB ribbons. In Proceedings of the 12th Symposium on Laser Technology - Progress and Applications of Lasers, Mil Univ Technol, Jastarnia, POLAND, Sep 25-27, 2018.
- Czyz, O.; Kusinski, J.; Radziszewska, A.; Liao, Z.Q.; Zschech, E.; Kac, M.; Ostrowski, R. Study of Structure and Properties of Fe-based Amorphous Ribbons after Pulsed Laser Interference Heating. *Journal of Materials Engineering and Performance* **2020**, *29*, 6277-6285. <https://doi.org/10.1007/s11665-020-05109-w>.
- Trexler, M.M.; Thadhani, N.N. Mechanical properties of bulk metallic glasses. *Progress in Materials Science* **2010**, *55*, 759-839. <https://doi.org/10.1016/j.pmatsci.2010.04.002>.
- Jia, J.; Wu, Y.; Shi, L.; Wang, R.; Guo, W.; Bu, H.; Shao, Y.; Chen, N.; Yao, K. Influence of Annealing Process on Soft Magnetic Properties of Fe-BC-Si-P Amorphous Alloys. *Materials* **2024**, *17*, 1447.
- Chaudhari, P.; Turnbull, D. Structure and properties of metallic glasses. *Science* **1978**, *199*, 11-21. <https://doi.org/10.1126/science.199.4324.11>.
- Bennett, C.H.; Polk, D.E.; Turnbull, D. Role of composition in metallic glass formation. *Acta Metallurgica* **1971**, *19*, 1295-&. [https://doi.org/10.1016/0001-6160\(71\)90064-2](https://doi.org/10.1016/0001-6160(71)90064-2).
- Löffler, J.F. Bulk metallic glasses. *Intermetallics* **2003**, *11*, 529-540. [https://doi.org/10.1016/s0966-9795\(03\)00046-3](https://doi.org/10.1016/s0966-9795(03)00046-3).
- Löffler, J.F. Recent progress in the area of bulk metallic glasses. *Zeitschrift für Metallkunde* **2006**, *97*, 225-233.
- Marin, P.; Vázquez, M.; Olofinjana, A.; Davies, H. Influence of Cu and Nb on relaxation and crystallization of amorphous FeSiB (CuNb) wires. *Nanostructured Materials* **1998**, *10*, 299-310.
- Lashgari, H.; Chen, Z.; Liao, X.; Chu, D.; Ferry, M.; Li, S. Thermal stability, dynamic mechanical analysis and nanoindentation behavior of FeSiB (Cu) amorphous alloys. *Materials Science and Engineering: A* **2015**, *626*, 480-499.
- Inoue, A.; Shen, B.L.; Takeuchi, A. Developments and applications of bulk glassy alloys in late transition metal base system. *Materials Transactions* **2006**, *47*, 1275-1285. <https://doi.org/10.2320/matertrans.47.1275>.
- Yoshizawa, Y.a.; Oguma, S.; Yamauchi, K. New Fe-based soft magnetic alloys composed of ultrafine grain structure. *Journal of Applied Physics* **1988**, *64*, 6044-6046.
- Hono, K.; Hiraga, K.; Wang, Q.; Inoue, A.; Sakurai, T. The microstructure evolution of a Fe₇₃. 5Si₁₃. 5B₉Nb₃Cu₁ nanocrystalline soft magnetic material. *Acta Metallurgica et Materialia* **1992**, *40*, 2137-2147.
- Hono, K.; Li, J.-L.; Ueki, Y.; Inoue, A.; Sakurai, T. Atom probe study of the crystallization process of an Fe₇₃. 5Si₁₃. 5B₉Nb₃Cu₁ amorphous alloy. *Applied surface science* **1993**, *67*, 398-406.
- Chrissafis, K.; Maragakis, M.; Efthimiadis, K.; Polychroniadis, E. Detailed study of the crystallization behaviour of the metallic glass Fe₇₅Si₉B₁₆. *Journal of Alloys and Compounds* **2005**, *386*, 165-173.

20. Zhang, Y.; Ramanujan, R. A study of the crystallization behavior of an amorphous Fe₇₇. 5Si₁₃. 5B₉ alloy. *Materials Science and Engineering: A* **2006**, *416*, 161-168.
21. Yoshizawa, Y.; Yamauchi, K. Fe-based soft magnetic alloys composed of ultrafine grain structure. *Materials Transactions, JIM* **1990**, *31*, 307-314.
22. Ohta, M.; Yoshizawa, Y. New high-Bs Fe-based nanocrystalline soft magnetic alloys. *Japanese Journal of Applied Physics Part 2-Letters & Express Letters* **2007**, *46*, L477-L479. <https://doi.org/10.1143/jjap.46.1477>.
23. Kulik, T. The influence of copper, niobium and tantalum additions on the crystallization of FeSiB-based glasses. *Materials Science and Engineering: A* **1992**, *159*, 95-101.
24. Kusinski, J.; Czyz, O.; Radziszewska, A.; Morgiel, J.; Ostrowski, R.; Strzelec, M.; Czyz, K.; Rycyk, A. Crystallization of FeSiB amorphous ribbons induced by laser interference irradiation. *Archives of Foundry Engineering* **2018**, *18*, 27-30. <https://doi.org/10.24425/122497>.
25. Buividas, R.; Mikutis, M.; Juodkazis, S. Surface and bulk structuring of materials by ripples with long and short laser pulses: Recent advances. *Progress in Quantum Electronics* **2014**, *38*, 119-156.
26. Tomita, T.; Kinoshita, K.; Matsuo, S.; Hashimoto, S. Effect of surface roughening on femtosecond laser-induced ripple structures. *Applied Physics Letters* **2007**, *90*.
27. Borowiec, A.; Haugen, H. Subwavelength ripple formation on the surfaces of compound semiconductors irradiated with femtosecond laser pulses. *Applied Physics Letters* **2003**, *82*, 4462-4464.
28. Cui, L.Y.; Men, H.; Makino, A.; Kubota, T.; Yubuta, K.; Qi, M.; Inoue, A. Effect of Cu and P on the Crystallization Behavior of Fe-Rich Hetero-Amorphous FeSiB Alloy. *Materials Transactions* **2009**, *50*, 2515-2520. <https://doi.org/10.2320/matertrans.M2009206>.
29. Herzer, G.; Buschow, K. Handbook of magnetic materials. *KHJ Buschow Elsevier Science Amsterdam* **1997**.
30. Warlimont, H.; Martienssen, W. *Springer Handbook of Materials Data*; Springer: 2018.
31. Kuhnt, M.; Marsilius, M.; Strache, T.; Polak, C.; Herzer, G. Magnetostriction of nanocrystalline (Fe,Co)-Si-B-P-Cu alloys. *Scripta Materialia* **2017**, *130*, 46-48. <https://doi.org/10.1016/j.scriptamat.2016.11.004>.
32. Shuja, S.Z.; Yilbas, B.S.; Momin, O. Laser repetitive pulse heating and melt pool formation at the surface. *Journal of Mechanical Science and Technology* **2011**, *25*, 479-487. <https://doi.org/10.1007/s12206-010-1208-4>.
33. Brygo, F.; Semerok, A.; Oltra, R.; Weulersse, J.M.; Fomichev, S. Laser heating and ablation at high repetition rate in thermal confinement regime. *Applied Surface Science* **2006**, *252*, 8314-8318. <https://doi.org/10.1016/j.apsusc.2005.11.036>.

Disclaimer/Publisher's Note: The statements, opinions and data contained in all publications are solely those of the individual author(s) and contributor(s) and not of MDPI and/or the editor(s). MDPI and/or the editor(s) disclaim responsibility for any injury to people or property resulting from any ideas, methods, instructions or products referred to in the content.